# Characterization of the robustness of SHM imaging techniques using the absolute error of localization

Jérémy Moriot, Nicolas Quaegebeur, Alain Le Duff, Patrice Masson

# Characterization of the robustness of SHM imaging techniques using the absolute error of localization

Jérémy MORIOT [1,2], Nicolas QUAEGEBEUR [1], Alain LE DUFF [2,3], Patrice MASSON [1]

[1] Groupe d'Acoustique de l'Université de Sherbrooke Sherbrooke (GAUS), 2500 boul. de l'Université, Sherbrooke, Canada J1K 2R1 Jeremy.moriot@gmail.com, Nicolas.quaegebeur@usherbrooke.ca, Patrice.masson@usherbrooke.ca
[2] ESEO, 10 Boulevard Jeanneteau, CS 90717, 49107 Angers, France alain.leduff@eseo.fr
[3] LUNAM University, LAUM, CNRS UMR 6613, Le Mans, France.

## Abstract

Guided waves-based imaging techniques have been studied for decades and have showed great potential for fast localization of defects on isotropic and anisotropic structures. In particular, pitch-catch techniques based on scattered waves allow inspection of large structures with a small number of actuators. In this paper, an approach is presented for characterizing the robustness of two imaging techniques for localizing a defect on an aluminium plate instrumented with three piezoelectric transducers, considering the absolute error of localization (AEL). This intuitive metric is useful for evaluating the probability of localization of a defect occurring on a structure where a critical zone is monitored. The robustness with respect to the distance between the transducers of the array and the level of noise in residual signals is studied. AEL values are mapped for several positions and sizes of the defect and a procedure for maximizing the ratio of correct localization over the grid is proposed.

**Keywords:** Structural Health Monitoring, piezoelectric embedded sensors, guided waves, image processing, defect characterization, aerospace

## 1. INTRODUCTION

Guided waves-based imaging have been studied for decades and have showed great potential for fast localization of defects on isotropic and anisotropic structures [1,2]. Among them, techniques based on scattered waves by a defect are cost-effective since it requires a small number of sensors for scanning large areas [2]. Nowadays, these techniques are mature enough for being implemented in a large-scale military or civil area. In accordance with the ARP6461 guidelines, probability of detection (PoD) curves are recommended for characterizing the ability of structural health monitoring (SHM) techniques to detect a defect [3]. A different empiric PoD curves approach is required with SHM techniques, because of the good reproducibility of acoustic signals when experimental conditions are stable. This contrast with classical non-destructive evaluation techniques (NDT) for which the human intervention is a factor of non-reproducibility. Then, the production of PoD curves requires a statistically representative number of samples instrumented in the same way [4] or a model-assisted procedure [5,6]. Moreover, the PoD characterizes only the ability of a technique for detecting the presence of a defect and does not consider its localization since movable transducer is inherent to standard NDT. For a certain structure being monitored, some areas are more critical than others, so the presence of a defect is has a variable impact regarding the structure integrity. In the present paper, the absolute error of localization (AEL) is first

presented as a tool for making a binary decision process in order to evaluate the criticality of the presence of a defect. Then, it is used for characterizing the robustness of the localization of two imaging techniques numerically and experimentally regarding the distance between the actuators of the array and the level of noise of the recorded signals. Finally, a procedure for maximizing the ratio of correct localization over the grid using AEL values is proposed.

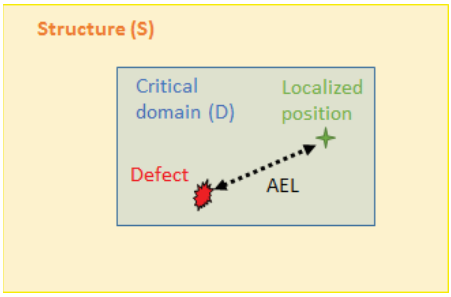


Figure 1: Illustration of the AEL.

### 1.1 Absolute Error of Localization (AEL)

In this paper, a structure (S) is considered on which a critical domain (D) exists, that has a particular geometry (it can be composed of one area or several separated areas). We assume that a defect has been detected and exists somewhere on the structure. We are interested in evaluating ability of an imaging technique to correctly localize the defect of a given size.

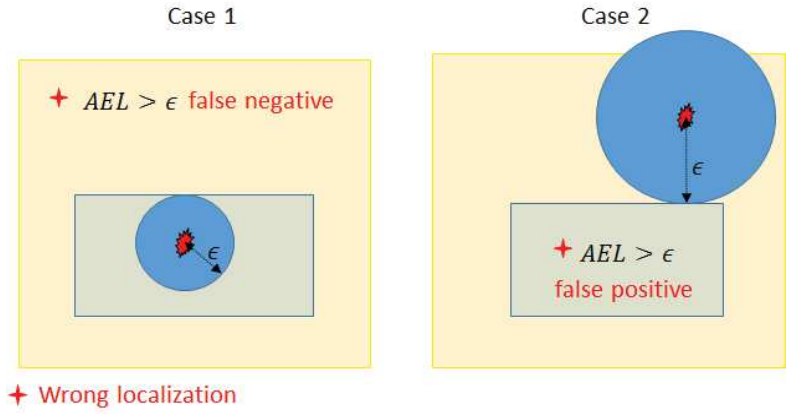


Figure 2: Illustration of the two different cases that can exist.

The metric that is used to locate the defect is the absolute error of localization (see Figure 1). It is simply the Euclidian distance between the defect location pointed by the imaging technique and its real position. A "correct localization" means that "the defect is localized in the domain (D) where it is actually located". Considering the AEL as the only metric upon which this evaluation is based and let $\epsilon$ be the maximal tolerance (maximum acceptable AEL value), the Figure 2 presents the two different cases that can exist:

- Case #1: the defect is located in the critical domain. If $AEL > \epsilon$, the imaging technique localizes it outside of the critical domain that corresponds to a false negative.

- Case #2: the defect is located outside of the critical domain. If $AEL > \epsilon$, the imaging technique localizes it in the critical domain that corresponds to a false positive.

In both cases, the correct localization corresponds to $AEL \leq \epsilon$.

### 1.2 Probability of localization

In the present paper, measurements are performed only once for each positions $(x, y)$ and size of defect $\phi$ that is enough for calculating localization ratios. A statistically representative number of measurements would allow to approximate the probability distribution of $AEL(x, y, \phi)$. Knowing the geometry of the critical domain that is monitored, the probability of localization as a function of the size (and eventually the kind) of defect to be localized can be expressed as:

$$PoL(\phi) = \int_C P\{AEL(x, y, \phi) \leq \epsilon(x, y)\} dx dy. \quad (6)$$

In this expression, $\epsilon(x, y)$ is the local tolerance that depends exclusively on the geometry of the boundary (or eventually multiple boundaries if several critical domains exist). Such an approach, coupled with an empiric-analytic model for Lamb waves generation and propagation can be employed for generating theoretical curves of probability of localization.

## 2. CHARACTERIZATION OF THE ROBUSTNESS OF IMAGING TECHNIQUES

### 2.1 Imaging techniques

An infinite aluminium plate of 1.54 mm thickness, instrumented with 3 piezoelectric transducers forming an equilateral triangle is considered, as it is represented in Figure 3.

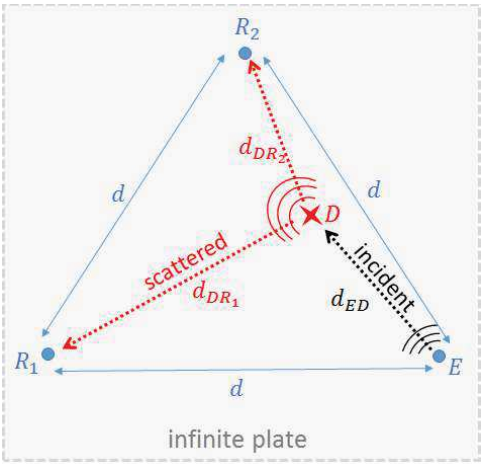


Figure 3: System configuration.

The AEL is used as a metric for evaluating the robustness of two imaging techniques based on scattered guided waves. Two imaging techniques based on scattered guided waves are employed. An acoustic signal is generated by an emitter (noted $E$), and recorded by the two

receivers (noted $R_1$ and $R_2$, respectively) after being propagated into the structure. If a defect (noted $D$) is present, a slight part of this acoustic wave is scattered by the defect.

Subtracting a baseline signal (performed on pristine structure) to the signal in presence of the defect gives the residual signal. If no significant environmental changes occurred between these two records, the residual signal characterizes only the defect. The residual signal $\mathbf{r}_{\mathrm{ER}}$ between each couple of emitter – receiver is then used to generate an image index $\boldsymbol{I}$ that is calculated for each pixel of coordinates $(x, y)$ of a grid. The general expression of the index is:

$$\boldsymbol{I} = \left| \sum_{\mathrm{E}} \sum_{\mathrm{R}} \Delta^{\mathbf{A}} \{\mathcal{H}(\mathbf{r}_{\mathrm{ER}})\} \right|. \tag{1}$$

In this expression, $\Delta^{\boldsymbol{A}}$ is the imaging process, that necessitates a library $\boldsymbol{A}(x, y, t)$ of signals corresponding to each pixel and each couple of emitter-receiver. $\mathcal{H}(\mathbf{r}_{\mathrm{ER}})$ denotes the Hilbert transform of the residual signal.

### 2.1.1 Delay-And-Sum with Dispersion Compensation (DAS-DC)

In this technique, an operation of compensation of the dispersion is first applied to the residual signal [7]. This operation necessitates to calculate the dispersion curves of Lamb waves of the material. Then, the classical delay-and-sum beamforming is applied to the compensated residual signal $\mathbf{r}^{\mathbf{c}}_{\mathrm{ER}}$. Eq. (1) is then expressed as:

$$\boldsymbol{I} = \left| \sum_{\mathrm{E}} \sum_{\mathrm{R}} \int_{-\infty}^{+\infty} \mathcal{H}(\mathbf{r}^{\mathrm{c}}_{\mathrm{ER}}).\, \delta\left( t - \left[ \frac{d_{EDR}}{c_g} + t_b \right] \right) dt \right|, \tag{2}$$

where $\delta(.)$ is the Dirac delta function, $d_{EDR}$ is the distance between the emitter, the defect and the receiver, $t_b$ is the half duration of the excitation signal, and $c_g$ is the group velocity of the considered mode.

### 2.1.2 Excitelet (Correlation-based)

In the Excitelet technique, the residual signal is correlated with a library of theoretical signals, called atoms, which correspond to propagated versions of the input signal for each pixel in the imaging space [2]. For this work, the pin-force model coupled to a propagation model was used to generate the atoms forming the library $\boldsymbol{A}$. This model takes into account the propagation of both $A_0$ and $S_0$ modes including the dispersion effect and the electro-mechanical impedance of the transducer, assuming a uniform shear stress profile below the transducer [8]. With this technique, the imaging index is:

$$\boldsymbol{I} = \left| \sum_{\mathrm{E}} \sum_{\mathrm{R}} \int_{-\infty}^{+\infty} \mathcal{H}(\mathbf{r}_{\mathrm{ER}}).\, \boldsymbol{A}(x, y, t) dt \right|, \tag{3}$$

where

$$\boldsymbol{A}(x,y,t) = \left( \int_{-\infty}^{+\infty} \boldsymbol{H}_{ER}(x,y,\omega) e^{-j\omega t}\, d\omega \right) * U(t). \quad (4)$$

In Eq. (4), $(*)$ denotes the convolution product, $\omega$ is the angular frequency, $U(t)$ is the input signal and $\boldsymbol{H}_{ER}(x,y,\omega)$ is the transfer function between the emitter, the defect (considered as a punctual omnidirectional reflector), and the receiver [8].

### 2.2 Presentation of the experiment

The system that is considered is a square 1.54 mm thick isotropic aluminium plate of 60 cm length on which three piezoelectric transducers PZT-5A of 0.5 mm thick and 5 mm diameter are bonded (see Figure 4). The transducers form an equilateral triangle and the distance between each pair of transducer is 20 cm. An absorbing paste is used for minimizing the acoustic reflections by the edges of the plate. A viscoelastic disc of 5 mm diameter on which a mass of 340 g is applied is used to simulate a reflector, and moved around 496 positions in turn on the plate. For each position, an image is generated and the AEL value is calculated. A sinusoidal Hann-filtered burst of 3.5 cycles at 175 kHz is generated by one emitter and recorded by the two others. This frequency is the theoretical natural frequency of amplification of the $A_0$ Lamb wave mode regarding the geometry and size of the emitter [8]. This procedure is repeated with another emitter, thus characterizing the three possible couples of emitter-receiver. The duration of the recording is 1 ms, the sampling frequency is 6 MHz, and measurements are averaged 300 times in order to increase the Signal-to-Noise Ratio (SNR) of the recorded data. A HP 33120A function generator and a Novo Electronics UA8200 amplifier are used for generating the burst. A NI-5105 acquisition device is used for recording the response voltage signal generated by the two other transducers and for synchronizing the generation and the acquisition.

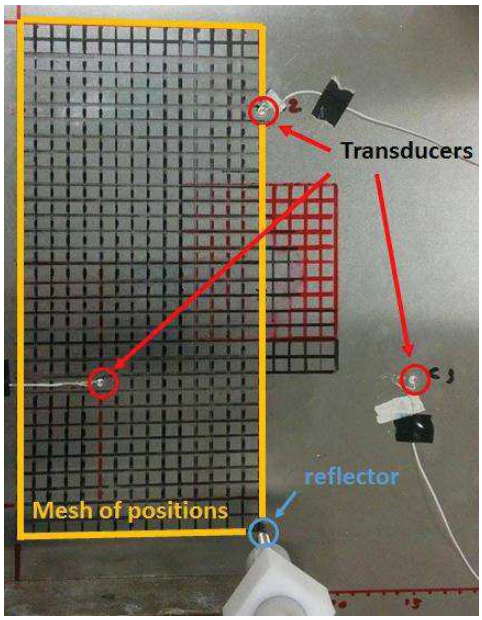


Figure 3 : Experimental setup.

### 2.3 Localization performance over the whole imaging domain

AEL values obtained with the DAS-DC and the Excitelet techniques, and corresponding to each of the 496 positions of the reflector, are mapped in Figure 5. A threshold of 20 mm is set for the maximum AEL. AEL values superior to 20 mm are then not represented. Values corresponding to abscissa $x = 1$ cm to $x = 15$ cm are obtained by symmetry with the values at abscissa $x = -1$ cm to $x = -15$ cm. It appears that AEL values are not uniform. Some positions, exhibiting a low AEL, lead naturally to a good localization. Rather, if the reflector is located at positions characterized by a high EAL value (typically exceeding 10 mm), false positive or false negative will more likely occur. Some of these unfavourable positions are located close to the transducers. An attenuation of the signal by the reflector in the vicinity of the corresponding transducer, leading to avoiding its contribution to the imaging can explain this effect. Also, the burst frequency was adapted in order to maximize the amplitude of the signal but not to maximize its interaction with the reflector. This last point will be investigated in section 2.5.

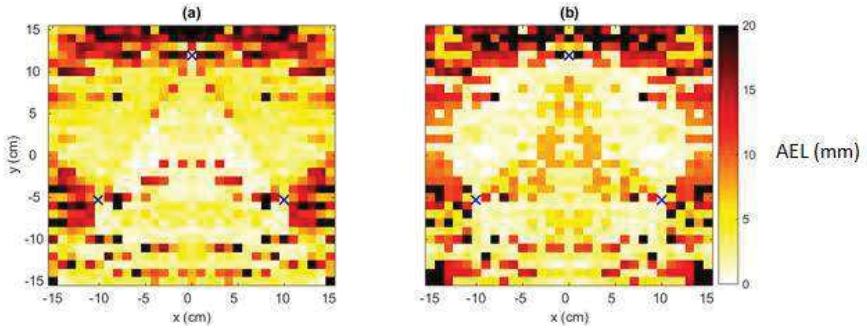


Figure 4: Maps of AEL values over the 496 positions of the experimental grid obtained with the DAS-DC technique (a) and the Excitelet technique (b). Blue crosses: sensors locations.

For a better interpretation of results presented in Figure 5, the ratio between the positions for which $AEL \leq \epsilon$ and the entire tested positions, called localization ratio (LR), is plotted as a function of $\epsilon$ in Figure 5. The LR value increases when the tolerance increases, which is an intuitive result. Despite some slight variations between the two curves in Figure 5, we see that the two techniques show similar performance for high $\epsilon$.

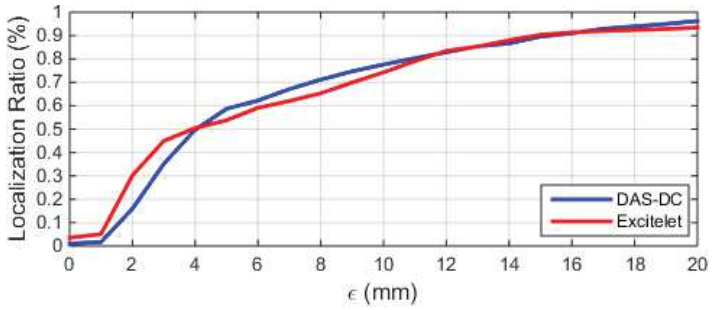


Figure 5: Ratio of correct localization versus the tolerance $\epsilon$.

For low $\epsilon$ values, the Excitelet technique shows better performance. Such a representation is useful for defining a threshold of maximum acceptable tolerance.

### 2.4 Numerical characterization of the robustness of the localization

In this section, AEL values are used to numerically characterize the robustness of the imaging techniques over the distance between the sensors (noted $d$ in Figure 3) and over the background noise. Results are presented in Figures 6 and 7, respectively.

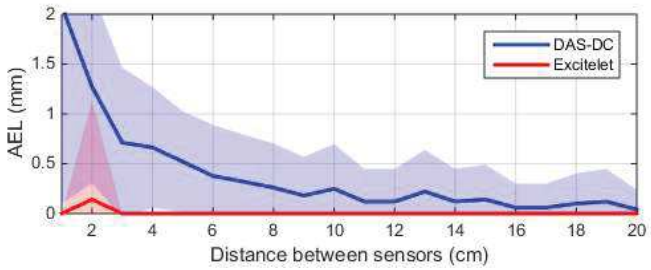


Figure 6: Simulated AEL mean value (solid line) and confidence interval (transparent area) versus the sensor spacing $d$.

Results shown Figure 6 are obtained numerically, by selecting 50 random positions over the grid and by calculating each AEL value, for various distances $d$ between the transducers. We can see that the two techniques are slightly, impacted by a variation of the sensor spacing, the maximum AEL mean is less than 0.2 mm with Excitelet and 2 mm with DAS-DC. Consequently, sparse or compact array can be used without degradation of the performance of the localization. One reflector position, showing an AEL equal to 0 in Figure 4, was selected for testing the robustness of the two techniques considering various noise level in the residual signal. A white Gaussian noise is added to the residual signal that corresponds to a Signal-to-Noise Amplitude Ratio (SNAR). The SNAR definition is:

$$SNAR = 20\log_{10}\left(\frac{max|s(t)|}{max|n(t)|}\right), \tag{5}$$

where $s(t)$ and $n(t)$ are the residual signal and the additional noise, respectively.

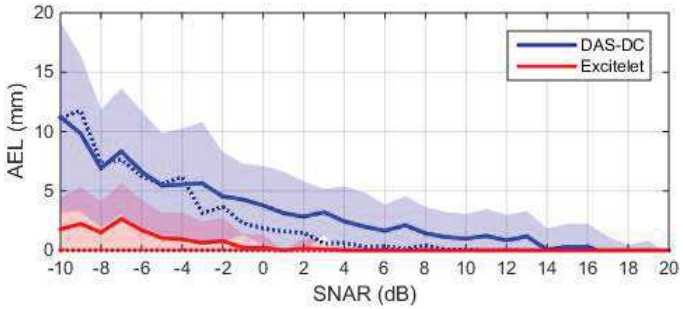


Figure 7: AEL versus SNAR obtained with the DAS-DC technique (blue) and the Excitelet technique (red); plain line: experimental mean value, transparent area: confidence interval, dotted line: numerical mean value.

This definition is more adapted than the classical SNR because it was observed that these two techniques were able to perfectly localize the reflector while the maximum of the residual signal, which corresponds to the peak of the $A_0$ mode, were still visible. In order to extract the mean value of the AEL and the confidence interval, this procedure is repeated 50 times for each SNAR value. Numerical results show that the DAS-DC technique is more sensitive

to the noise than the Excitelet technique, which gives always an AEL equal to 0. Experimental results confirm this observation. Even with a SNAR of -10 dB, the DAS-DC technique exhibits an AEL mean equal to 10 mm which still corresponds to a correct localization. Globally, the two techniques appear to be very robust to the background noise.

### 2.5 AEL-based optimal frequency selection for multiple size defect localization

The two imaging techniques are now employed for localizing a circular viscoelastic reflector with diameter varying from 1.8 mm to 6.35 mm, as it is shown in Figure 8.

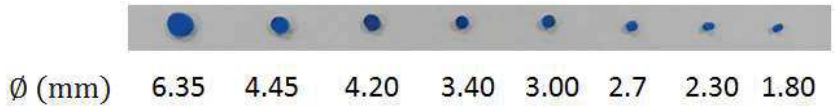


Figure 8: Reflectors with diameter varying from 1.8 mm to 6.35 mm.

The reflector is set at 28 regularly spaced positions over the grid on the plate presented in Figure 4.

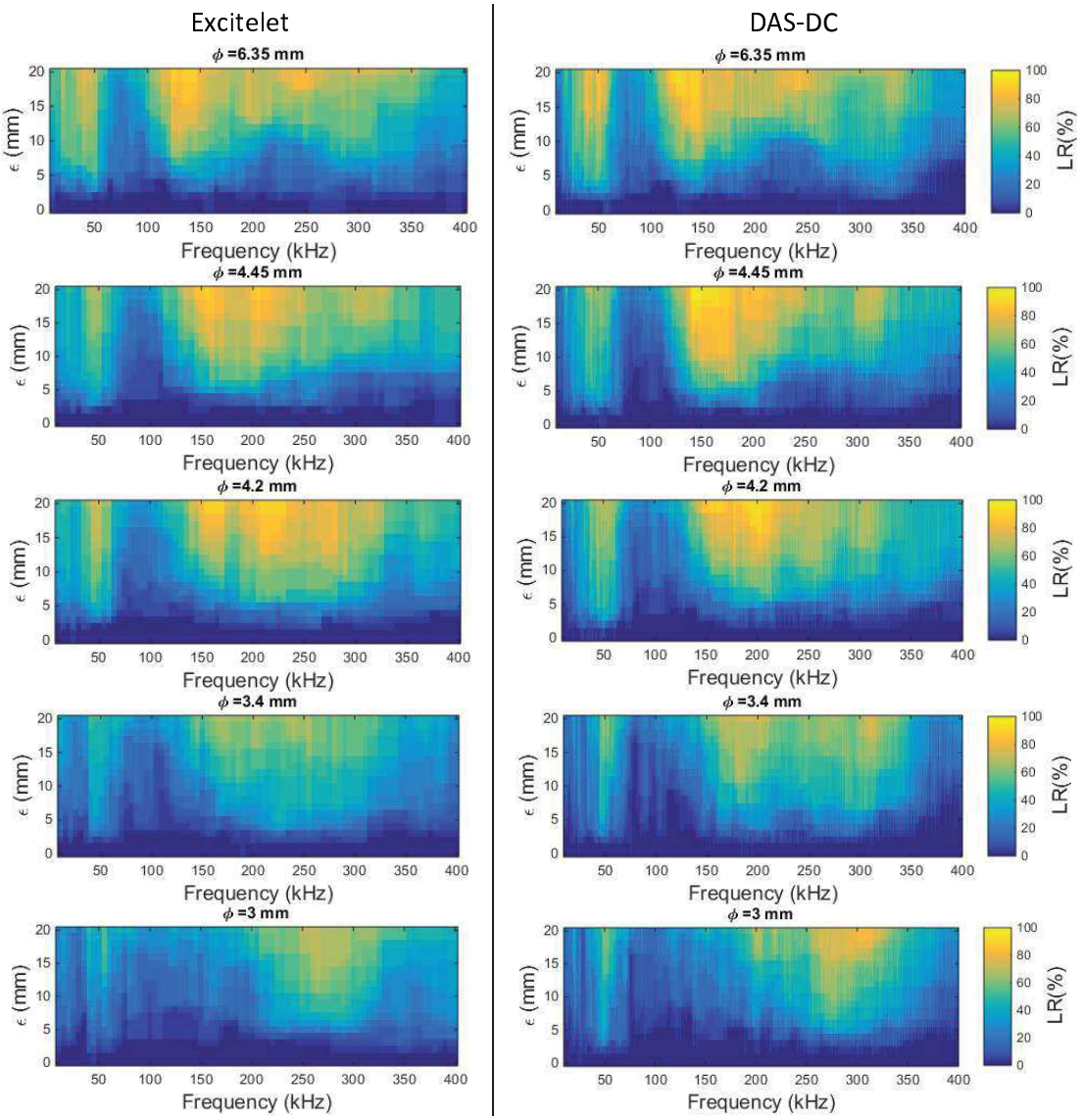

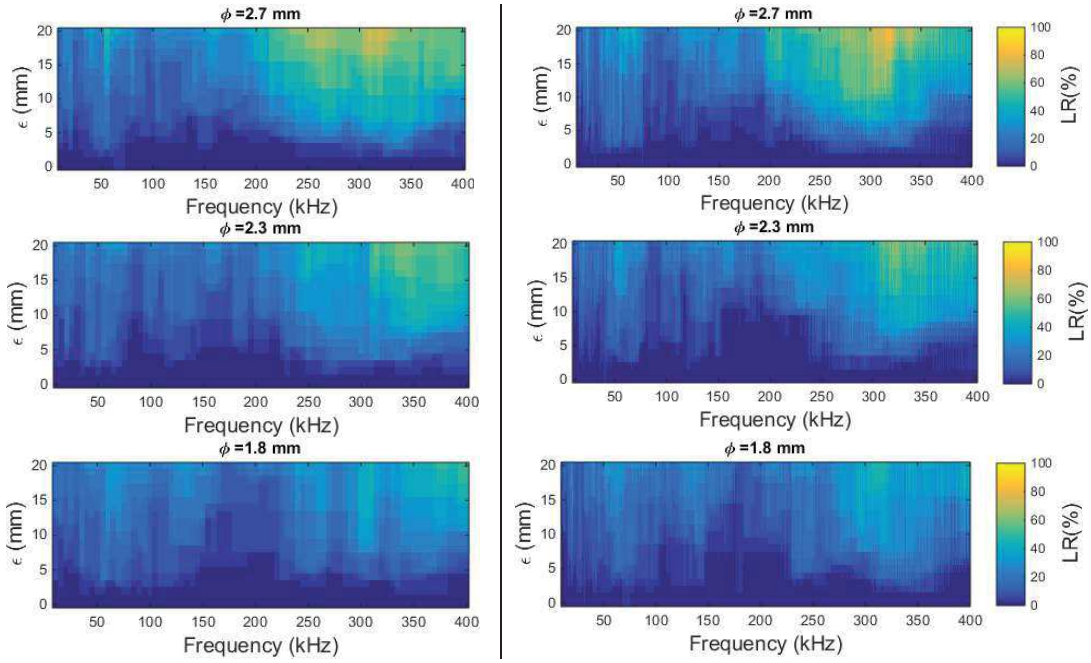


Figure 9: Localization ratio of positions showing an AEL$\leq \epsilon$ versus the frequency of the burst (in abscissae).

We are interested in determining the frequency that optimizes the LR value as a function of the size of the reflector. The Figure 9 presents, for the two techniques, the LR values obtained experimentally with the 8 sizes of reflector versus the tolerance $\epsilon$ (in ordinates) and for a burst at a frequency varying from 10 kHz to 400 kHz (in abscissa). We already indicated in Figure 5 that the LR increases with $\epsilon$. For the two techniques, the maximum LR value that can be obtained varies with the burst frequency.

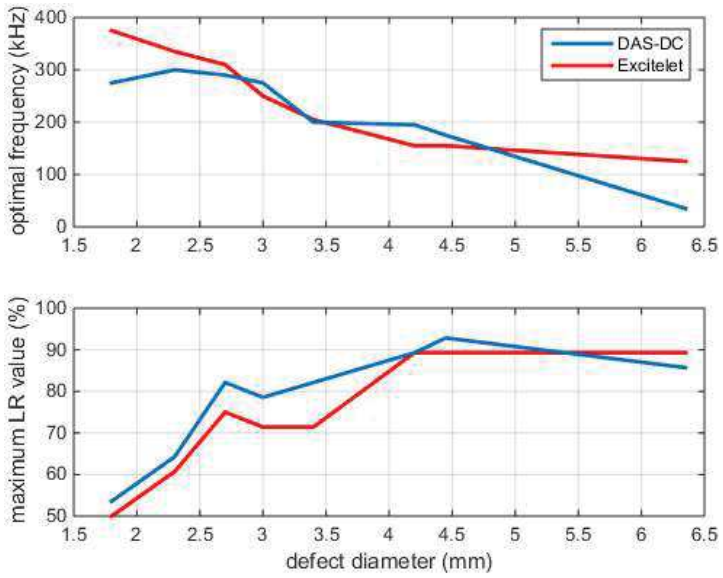


Figure 10 - Optimal selected frequency and maximum value of the localization ratio associated versus the defect diameter.

Some frequency ranges appear to be more adapted for maximizing the LR which increases as the size of the defect decreases, which is an intuitive behaviour. Also, the maximum LR

value decreases when the size of the reflector decreases. For large defects, the difference between the signal and the baseline is notable. But for small defects, the scattered part of the signal is small. Then, the residual signal tends to the noise, thus degrading the localization. This effect is clearly visible in Figure 10, which presents the burst frequency that maximizes the LR value, called optimal frequency, for $\epsilon = 20\ mm$ and this maximum LR. A similar behaviour is observed with the two techniques.

## 3. CONCLUSION

In this paper, the performance of two guided waves-based techniques that consider the signal scattered by a defect on an aluminium plate was characterized using the Absolute Error of Localization (AEL) between the defect and the location spotted by the method. This simple and intuitive metrics was mapped for a grid of positions of a reflector. This approach is useful for determining the ratio of positions for which the localization is correct with respect to a maximum tolerance. The AEL was employed for characterizing the robustness of the techniques as a function of the distance between the transducers of the array and of the background noise. Finally, it was shown that the maximum LR value that can be expected is a function of the exciting burst frequency, which depends of the size of the defect. Also, this maximum LR value decreases when the size of the defect decreases because a smaller fraction of the energy is scattered. This paper focuses on the use of the AEL as a metric for characterizing the performance of guided waves imaging techniques. In a future work, a model-assisted procedure will be employer for defining the AEL as a probability distribution and for generating curves of probability of localization.

## Acknowledgement

This study has been conducted with the financial support of Le Mans Acoustics Institute (LMAc). The authors would also like to acknowledge the Natural Sciences and Engineering Research Council of Canada (NSERC).

## References

[1] Z. Su, L. Ye and Y. Lu. Guided Lamb waves for identification of damage in composite structures: A review. Journal of Sound and Vibration, **295**(3-5), 753-780, 2006.

[2] N. Quaegebeur, P. Masson, D. Langlois-Demers, et al. Dispersion-based imaging for structural health monitoring using sparse and compact arrays. Smart Material and Structures. **20**(2), 025005, 2011.

[3] SAE International. Guidelines for implementation of structural health monitoring on fixed wing aircraft, 2013.

[4] V. Janapati, F. Kopsaftopoulos, F. Li, et. Al. Damage Detection Sensitivity Characterization of Acousto-Ultrasound-based SHM techniques. Structural Health Monitoring, 2016 (in press).

[5] A. C. Cobb, J. Fisher and J. E. Michaels. Model-Assisted Probability of Detection for Ultrasonic Structural Health Monitoring. Proceedings of the 4th European-American Workshop on Reliability of NDE, Berlin, Germany, 2009.

[6] G. Jarmer and S. Kessler. Probability of Detection Assessment of a Guided Wave Structural Health Monitoring System. Proceedings of the International Workshop on Structural Health Monitoring, Stanford (USA), 2015.

[7] P. D. Wilcox. A rapid signal processing technique to remove the effect of dispersion from guided wave signals. IEEE Transaction on Ultrasonics Ferroelectrics and Frequency Control. **50**(4), 419-427, 2003.

[8] A. Raghavan, C. E. S. Cesnik. Finite-dimensional piezoelectric transducer modelling for guided wave based structural health monitoring. Smart Material and Structures. **14**(6), 1448-1461, 2005.